JOURNAL OF AIRCRAFT
Vol. 41, No. 1, January–February 2004

Supercritical Airfoil Design for Future High-Altitude Long-Endurance Concepts

Kasim Biber*
Istanbul Technical University, 34870 Istanbul, Turkey
and
Carl P. Tilmann†
U.S. Air Force Research Laboratory, Wright–Patterson Air Force Base, Ohio 45433-7542

The design and analysis is presented of a new laminar flow airfoil for a future high-altitude long-endurance aircraft that has an operational condition at supercritical speeds. The XFOIL and MSES computational codes were used to design, modify, and analyze the airfoil. The airfoil has enough thickness and performance to meet the requirements set for one of the U.S. Air Force Research Laboratory's SensorCraft concepts: a joined-wing configuration with a diamond shape in planform and front views. This SensorCraft concept's geometry and operational altitudes and speeds were used to determine the airfoil design conditions. The airfoil has a drag bucket over a large range of lift coefficients. Boundary-layer transition location is at about 60% chord upper surface and 70% chord lower surface and is characterized by a laminar separation bubble, which decreases in size with increasing angle of attack. Sensitivity studies were carried out to investigate the effects of Reynolds number and Mach number, along with boundary-layer transition parameters. Further experimental work needs to be performed to validate the design.

Nomenclature

a	=	freestream speed of sound
C_D	=	airfoil section drag coefficient
C_L	=	airfoil section lift coefficient
C_M	=	airfoil section moment coefficient
C_P	=	pressure coefficient, $(p - p_\infty)/\frac{1}{2}\rho V^2$
c	=	chord
M	=	freestream Mach number, V/a
M_D	=	drag divergence Mach number
M_R	=	reduced Mach number, $M\sqrt{C_L}$
N_{cr}	=	critical amplification ratio
Re	=	chord Reynolds number, $\rho V c/\mu$
Re_R	=	reduced Reynolds number, $Re\sqrt{C_L}$
S	=	wing area
V	=	freestream speed
x_{tr}	=	transition location
α	=	angle of attack
μ	=	freestream viscosity
ρ	=	freestream density

Introduction

THE U.S. Air Force Research Laboratory (AFRL) has been identifying feasible vehicle concepts and aerodynamic technology development requirements for a new class of high-altitude long-endurance (HALE) concept vehicles known as SensorCraft. SensorCraft is conceived as an unmanned air vehicle system performing command, control, detection, identification, tracking, relay, and targeting functions for very long durations at extended ranges.[1,2] It is the airbreather component of a fully integrated intelligence, surveillance, and reconnaissance (ISR) enterprise that cohesively integrates air, space, and ground components of the entire ISR system (Fig. 1). This AFRL multidirectorate shared-vision program combines critical vehicle airframe, propulsion, sensor, flight, and information technologies into a highly responsive platform concept to provide persistent detection and surveillance of mobile, hidden targets. In addition to omnidirectional multispectral sensing, a primary mission goal is to increase greatly endurance with respect to existing platforms. Loiter times of 42 h at a 2000-n miles (3704 km) range have been set as goals.

Several candidate aircraft and propulsion configurations are under consideration to determine the best tradeoff between endurance, altitude, engine efficiency, and power generation. Concepts being considered include conventional wing–body–tail, flying wing, and joined-wing configurations. Each of these configurations brings with it a host of technical challenges that is driving technology investments at AFRL. The configurations and their aerodynamic performance are constrained by a host of antenna size, power, and field-of-view requirements, while demanding extreme levels of structural and aerodynamic efficiency, which have major impacts on vehicle size and cost. One of the greatest challenges facing the designers is the integration of the large antenna apertures required for lower frequency operations into the airframe. These lower frequency bands of operation would enable the SensorCraft to provide a foliage penetration radar capability, a key sensory mode aimed at defeating extremely difficult camouflaged, concealed, and deceived (CC&D) targets.

Whereas the concepts vary in many respects, they all share the common operational theme of ultralong endurance wide-area coverage at very high altitude. This results in the majority of flight operations at critical cruise Mach numbers and low Reynolds numbers. The long-endurance flight capability requires the aircraft to have maximum aerodynamic efficiency and minimum fuel consumption, as illustrated by their prominence in the Breguet endurance equations. For various reasons, primarily antenna integration, the aircraft may also require relatively thick wings. Because of these factors, it is likely that basing the wing designs on existing airfoil section will provide sub-optimal performance. Thus, it becomes necessary to develop a unique class of airfoils to use as the baseline for further development efforts.

The airfoil development reported here was aimed at developing a new airfoil for the future SensorCraft concepts that has the

Presented as Paper 2003-1095 at the 41st Aerospace Sciences Meeting and Exhibit, Reno, NV, 6 January 2003; received 6 March 2003; revision received 10 June 2003; accepted for publication 11 June 2003.

*Engineering Consulting, Karliktepe Mah, Serap Sok, Number 4/10, Istanbul, Turkey; kxbiber@yahoo.com. Senior Member AIAA.

†Senior Aerospace Engineer, Air Vehicles Directorate, AFRL/VAAA, Building 45, 2130 8th Street. Associate Fellow AIAA.

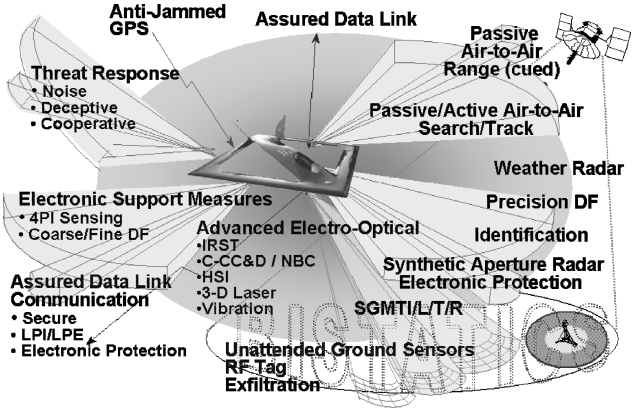

Fig. 1 SensorCraft role in the ISR enterprise (from Ref. 1).

maximum possible thickness and the best polar performance through supercritical speeds and at relatively low Reynolds numbers due to high-altitude loiter objectives. This paper outlines the computational design and analysis methods and procedures used in the development. The specific configuration chosen for sizing was a joined-wing concept developed to focus in-house technical assessment efforts[3] at AFRL. This type of SensorCraft has been the subject of many assessment and design efforts,[4,5] including aerodynamic weight estimation[6] and aeroelastic design.[7] It has also been the subject of linear aerodynamic design optimization studies[8,9] and planform modifications.[10] Although it is only one of the SensorCraft concepts being developed, the label SensorCraft will refer to this configuration for the remainder of this paper.

Airfoil Design Conditions

A baseline configuration has been established for the SensorCraft mission that accomplishes the necessary ISR tasks at some 65,000-ft cruise altitude and Mach number of 0.6. These baseline aircraft data are used here to determine the airfoil flow parameters such as reduced Mach and Reynolds number[11]:

$$M_R = M\sqrt{C_L} = \{(2/\gamma)[(W/S)/p]\}^{\frac{1}{2}}$$

$$Re_R = Re\sqrt{C_L} = [(2\rho/\mu^2)(W/AR)]^{\frac{1}{2}}$$

These constant lift flow parameters are more useful in evaluating the airfoil performance than the conventional Mach and Reynolds numbers because they remain the same as aircraft undergoes trim changes for a fixed altitude and vehicle weight.

Figure 2 shows a variation of the reduced Mach M_R and Reynolds number Re_R with altitude for the future SensorCraft concept. The variation is also shown in Table 1. The solid lines (Fig. 2) are for the maximum fuel loading when the aircraft is at takeoff gross weight (75,000 lb). The dashed lines are for when the aircraft is at the end of its long-loiter and most of the fuel has been expended (40,000 lb). For the maximum weight case, Re_R decreases to 3.477×10^6 as M_R increases to 0.606 as the vehicle climbs to an altitude of 65,000 ft, corresponding to the primary design condition for the airfoil. The fuel-burned case shows the sensitivity of the reduced Mach and Reynolds number parameters to wing loading, which is discussed later in the paper.

An empirical relation, given by Torenbeek[12] for symmetrical airfoils at zero lift is used as a rough estimate to find a relationship between the design Mach number and the airfoil maximum thickness, as shown in Fig. 3. The effect of 35-deg sweepback angle is included in calculations. As a priori knowledge, the SensorCraft mission requires an airfoil as thick as 20% chord. This much thickness corresponds to a critical design Mach number of 0.7, not counting the effects of camber or lift. The cruise Mach number of 0.6 seems to be reasonable to be a target on-design for the SensorCraft airfoil. Notice that the sweep back angle of 35-deg increases the critical design Mach number for the airfoil. However, the airfoil

Table 1 Reduced Mach and Reynolds numbers for SensorCraft takeoff and fuel-burned weight conditions

	Takeoff		Fuel burned	
Altitude, ft	M_R	Re_R	M_R	Re_R
10,000	0.172	9.18×10^6	0.125	6.71×10^6
50,000	0.421	4.96×10^6	0.307	3.62×10^6
55,000	0.478	4.43×10^6	0.349	3.24×10^6
60,000	0.535	3.90×10^6	0.391	2.85×10^6
65,000	0.606	3.47×10^6	0.444	2.54×10^6
70,000	0.680	3.04×10^6	0.497	2.22×10^6
75,000	0.771	2.70×10^6	0.563	1.97×10^6

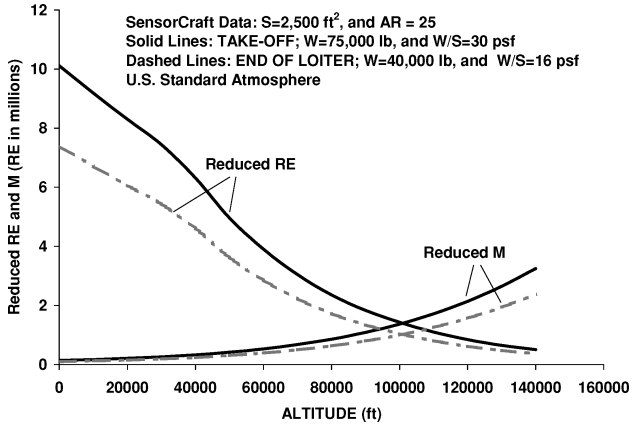

Fig. 2 Variation of reduced Mach and Reynolds numbers with altitude for takeoff maximum and fuel-burned weight conditions of the SensorCraft concept studied.

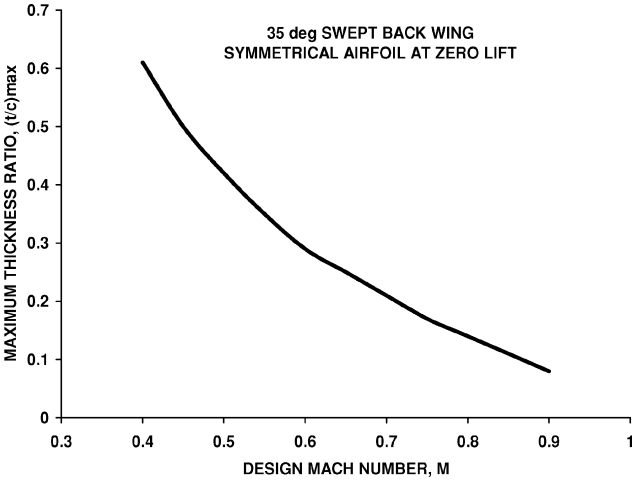

Fig. 3 Estimated thickness ratio variation with design Mach number for a symmetrical airfoil at zero lift including the effects of 35-deg sweepback wing.

should be evaluated at the design as well as off-design conditions to understand the effects of low and high altitudes on the airfoil performance, including the effects of supercritical flow that the airfoil would encounter at very high altitudes.

Airfoil Design Tools

The design effort included the use of XFOIL and MSES airfoil design and analysis programs (developed by M. Drela at Massachusetts Institute of Technology). Each program is menu driven and has user's guide describing its use and capabilities. XFOIL, version 6.94, is used for subsonic isolated airfoils, whereas the MSES, version 2.8, may be used for both single- and multi-element airfoils. XFOIL uses a combination of an inviscid panel solution coupled with a two-equation integral boundary layer through a surface transpiration

model, with added Kármán–Tsien compressibility correction. The boundary layer and wake are described with a two-equation lagged dissipation integral boundary formulation and an envelope e^N transition criterion. The airfoil surfaces admit a solid-body boundary condition in the direct analysis mode and a prescribed pressure boundary condition in the inverse-design mode. The overall system is solved using a full Newton method. MSES couples the same two-equation integral boundary-layer method with an Euler solver through the displacement thickness.[13,14]

Boundary-layer transition for both codes is predicted by a simplified version of the e^N method called the envelope method, as described in Ref. 14. Instead of tracking the Tollmien–Schlichting wave amplitudes for many individual frequencies, as in the e^N method, the envelope method determines for each surface point the amplitude of whatever frequency happens to be the most amplified at that point. This is a great simplification, but involves some approximations that have the greatest impact in flows where the parameter varies rapidly. The validity of the results of the envelope method can be easily checked in MSES by plotting amplitude of both the envelope as well as the amplifications for individual frequencies that would have been predicted by the e^N method. Ideally, the envelope curve just touches the largest of all of the individual frequency curves at each location. Any deviation from this ideal usually lies within uncertainty in the specified critical amplification factor N_{cr}.

New SensorCraft Airfoil Development

Such high performance airfoil development has been the subject of some other efforts at AFRL. One of them has aimed at developing and validating a family of airfoils, namely, the global range airfoil for laminar flow (GRALF) for global range transports.[15,16] The GRALF airfoil has relatively low maximum lift coefficient and a low drag bucket near zero-lift line, designed for transonic speeds. The low-drag feature is obtained by having a large extend of natural laminar flow on the airfoil surface. There is also relatively low speed, but higher lift Natural Laminar Flow (NLF) airfoils developed primarily for general aviation applications.[17,18] As a starting point for the present study, polar performance of these airfoils as well as others was analyzed for comparison.

Figure 4 shows a comparison of the surface pressure distributions of these two airfoils scaled to the same 15% chord thickness and at the same incompressible flow conditions at 4 deg of angle of attack. The performance data are presented for lift coefficients ranging from 0.5 to 1.0 for GRALF and from 0.5 to 1.5 for the NLF airfoil. For both airfoils, there is a large amount of laminar flow at low-lift coefficients, but it decreases rapidly on upper surface, although at relatively higher angle of attack for the NLF, with the increase of lift coefficient. The transition location on the lower surface of airfoils has a tendency to move downstream with increase of lift coefficient. The long run of laminar flow is a desirable feature for low-drag airfoil performance, so long as the shorter pressure recovery region does not cause abrupt boundary-layer separation, as is the case for some overly aggressive laminar airfoil designs.

The SensorCraft is envisioned to have extremely long endurance at high altitudes, requiring its wing to be as aerodynamically efficient as possible. The primary requirements for the wing section considered in this study included near 20% chord maximum thickness, over 50% chord laminar flow, low pitching moment, and operations at relatively high Mach and low Reynolds numbers. The large thickness requirement stems from the desire to integrate a large low-frequency antenna in each wing. A compromise was made among all of the requirements to increase the airfoil thickness while maintaining a high L/D ratio with large drag bucket at high-lift, high-speed, and low Reynolds number conditions. Surface pressure distribution or surface geometry was changed in mixed or inverse design modules of the XFOIL software to meet the design objectives. The interactive and iterative work resulted in a new 19.62% thick airfoil for the SensorCraft airfoil, as shown in Fig. 5. This new airfoil was designated SensorCraft root 20% thick-version A (SCR20–A).

Figure 6 shows the surface pressure distributions of the new airfoil at section lift coefficients ranging from 1.0 to 1.5. Figure 6a

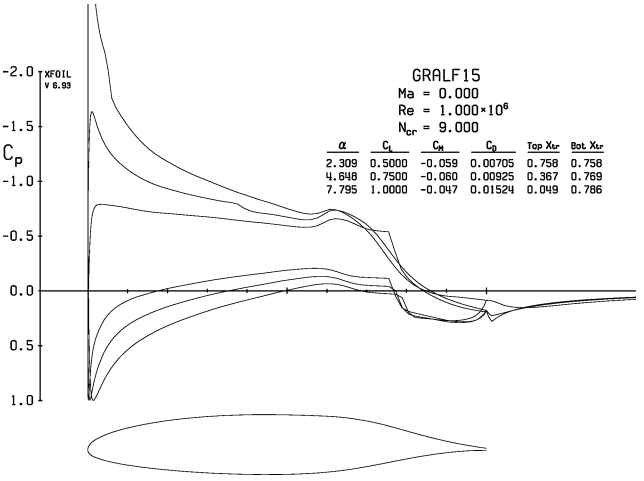

a) 15% thick GRALF airfoil for lift coefficients from 0.5 to 1.0

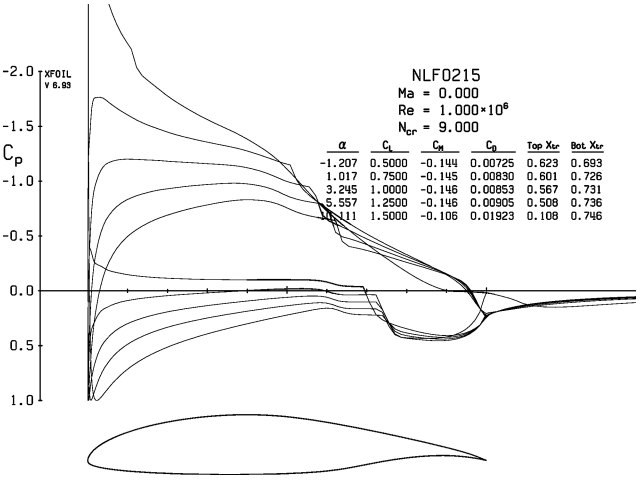

b) 15% thick NLF0215 airfoil for lift coefficients from 0.5 to 1.5

Fig. 4 Comparison of computed (XFOIL) surface pressure distribution at $\alpha = 4$ deg, $Re = 1 \times 10^6$, incompressible flow.

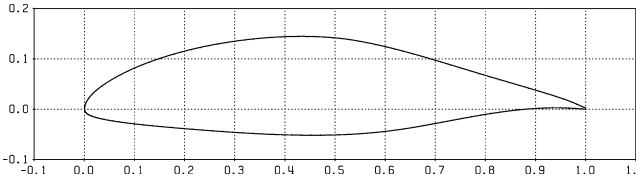

Fig. 5 Geometric view of the new 19.62% thick SCR20-A airfoil.

shows a comparison of viscous (solid lines) and inviscid (dotted lines) solutions obtained from XFOIL at $C_L = 1$. The inviscid solution produces smoother and higher values of surface pressures compared to the viscous case. As the boundary layer transitions to turbulent flow, there is a short flatness and then a sharp decrease of suction pressures. The behavior of surface pressure at the transition location suggests that the flow produces a transitional-type short bubble before the Stratford-type pressure recovery on the airfoil upper surface. The extent of laminar boundary layer is characterized by this type of transitional separation bubble, present at high subsonic Mach and relatively low Reynolds number flows. As seen in Fig. 6b, the transitional bubble decreases in size as the lift coefficient increases and almost disappears at the lift coefficient of 1.5, which is very close to airfoil stall. At the near-stall lift coefficient, the laminar flow extends to 55% chord location for the new SCR20-A airfoil, significantly high compared to compared to 10% chord location for the NLF airfoil presented in Fig. 4.

Because of its quick turnaround time, the XFOIL code was often used to analyze the airfoil performance. Figure 7 shows a

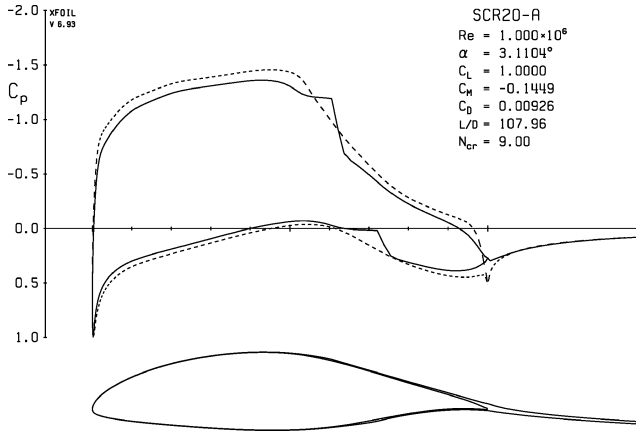

a) $C_L = 1$: ——, viscous solution and - - - -, inviscid solution

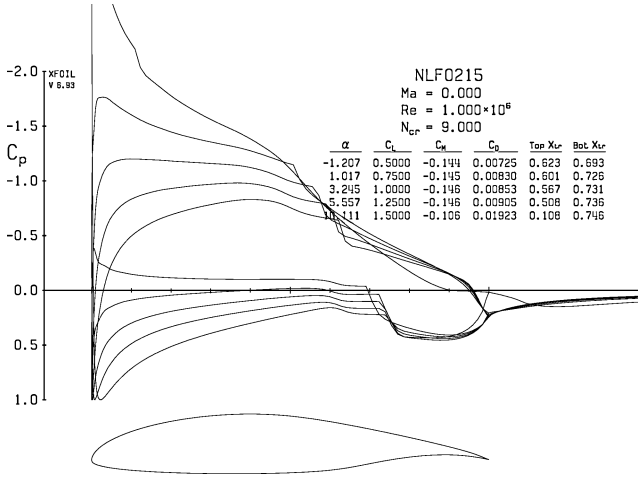

b) Performance data for C_L from 0.5 to 1.5

Fig. 6 Computed (XFOIL) surface pressure distribution for the SCR20-A airfoil at $Re = 1 \times 10^6$, incompressible flow.

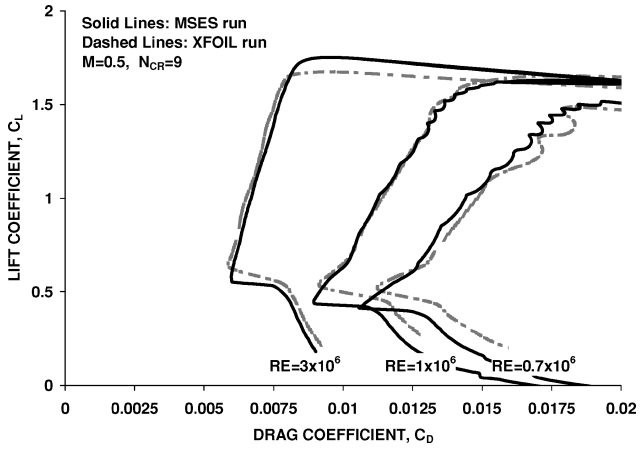

Fig. 7 Polar comparison of XFOIL and MSES runs at Mach 0.5 for Reynolds numbers of 0.7, 1, and 3×10^6, $N_{cr} = 9$.

comparison of the polar data obtained from the XFOIL and MSES codes at relatively low Reynolds numbers of 0.7, 1, and 3×10^6. The comparison was made at Mach number of 0.5 because of XFOIL's operation at subcritical speeds. The trends are the same for both codes, but there is little discrepancy at the high and low ends of the drag bucket. This is possibly due to the MSES code's more accurate simulation of supercritical compressibility and the resultant flow separation. The low Reynolds number design methods could be applicable to transonic speeds because the flow transition on airfoils is not affected by the increases of Mach number.[11] That is why

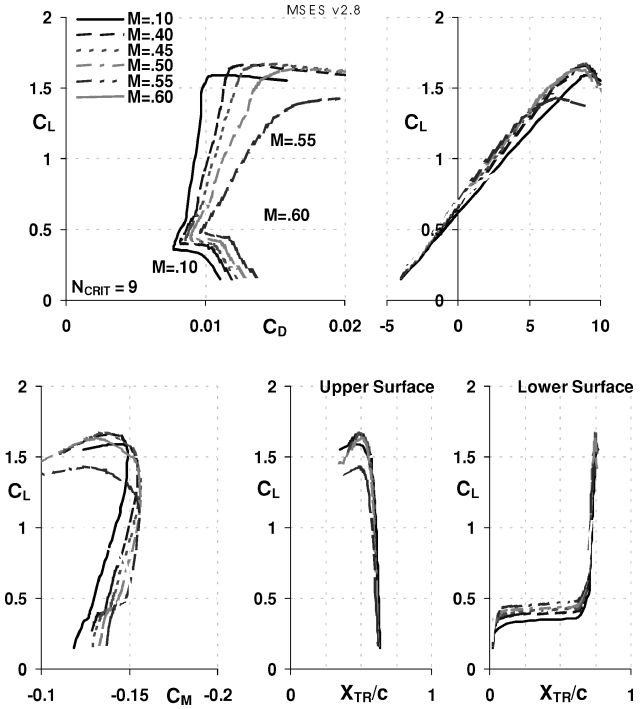

Fig. 8 Computed (MSES) airfoil performance showing the effects of Mach number on lift, drag, and pitching moment characteristics with Mach sweep from 0.1 to 0.60 at $Re = 1 \times 10^6$ and $N_{cr} = 9$.

compressibility effects should not make the codes differ from each other. The supercritical speeds, however, make a difference in design and off-design performance of airfoils. This present work relies on the MSES code more than the XFOIL because of its use of an Euler solver for the inviscid part of the flowfield.

Figure 8 shows a typical airfoil performance plot obtained with MSES at $Re = 1 \times 10^6$ and $N_{cr} = 9$. The slope of the linear portion of drag bucket ($\partial C_L / \partial C_D$) decreases with increasing Mach number. This effect is significant at Mach 0.60, probably due to the effects of shock formation on airfoil surfaces at supercritical speeds. The drag bucket has an upward shift, maximizing the lift coefficient at Mach number of about 0.45. The maximum C_L decreases at higher Mach numbers, due to shock formation and the associated flow separation. The airfoil produces a desirable maximum lift coefficient of about 1.67 at the moderate Mach numbers. The good airfoil performance is mainly due to the extensive laminar flow predicted at about 60% chord upper and 70% chord lower surface locations, as evidenced in free-transition locations of Fig. 8. The magnitude of the pitching moment increases almost linearly over a significant range in angle of attack (remaining at a relatively low negative value) and decreases near stall. The airfoil polar characteristics are probably better explored in Fig. 9, with a comparison of Reynolds number of 1×10^6 with 3×10^6 at Mach numbers of 0.55 and 0.60. Increasing Reynolds number has the effect of decreasing drag coefficient and increasing lift-curve slope and maximum lift coefficient, as expected. The large difference in drag coefficient is, however, also attributed to the size of laminar separation bubble, which decreases in size with increases in Reynolds number, as observed from surface pressure distributions. This also increases the maximum C_L for the $M = 0.55$ case.

One of the main objectives of airfoil design is to be able to obtain the highest possible drag divergence Mach number M_D, the Mach number for the onset of the dramatic increase in wave drag at a given lift coefficient, for a given maximum thickness ratio and wing sweepback. With this objective in mind, the MSES code was run with the Mach sweep option, and the airfoil drag was monitored. Figure 10 shows a drag divergence plot including a separate view of the wave drag contribution at high speeds at Reynolds number of 3×10^6. The solid lines are for fixed $\alpha = 2$ deg, and dashed lines are for fixed $C_L = 1$. As M reaches about 0.58, the drag coefficient starts diverging progressively from its profile value due

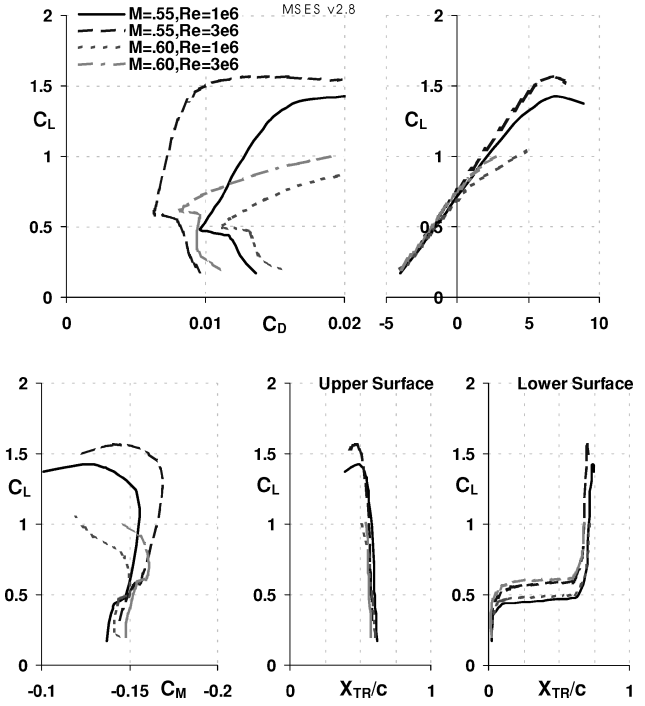

Fig. 9 Computed (MSES) airfoil performance showing the effects of Reynolds number on lift, drag, and pitching moment characteristics at $Re = 1$ and 3×10^6, Mach numbers of 0.55 and 0.60, and $N_{cr} = 9$.

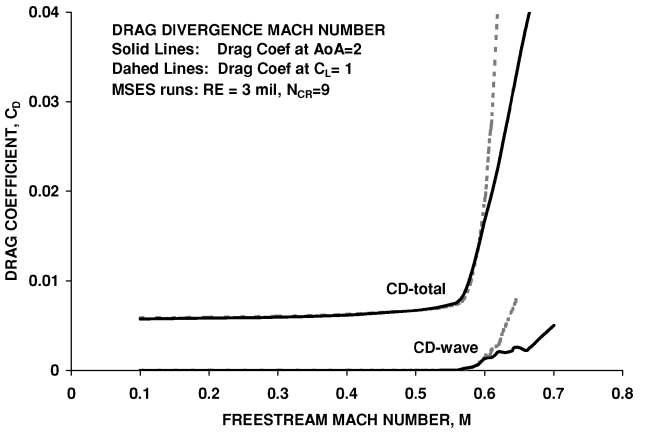

Fig. 10 Computed (MSES) total drag and wave drag variation (and divergence) $Re = 3 \times 10^6$ and $N_{cr} = 9$, with Mach number: ——, fixed $\alpha = 2$ deg and - - - -, $C_L = 1$.

to the increased compressibility effects. The drag increase is more pronounced for the fixed C_L case than that for the fixed angle-of-attack case at the transonic regime because the code maintains the requested C_L by further increasing α, leading to yet more severe shock-induced boundary-layer separation and corresponding loss of lift. It is, however, desirable to have the smallest possible initial rate of drag increase beyond M_D because the best cruise performance is obtained at a Mach number possibly 0.02–0.03 excess of M_D (Ref. 12).

Figure 11 shows the variation of C_L with Mach number for a fixed $\alpha = 2$ deg, as well as the variation in α with Mach number required to maintain a fixed $C_L = 1$. The fixed-α lift coefficient continues to increase with Mach number to its maximum value of 1.05 at Mach number of 0.57. Beyond this maximum, lift coefficient decreases rapidly due to the shock formation and related flow separation from the airfoil upper surface. The α required to maintain a fixed C_L of 1.0 decreases with increasing Mach number to a minimum value of 1.68, and then it shows a dramatic increase beyond the lift-divergent Mach number of 0.57.

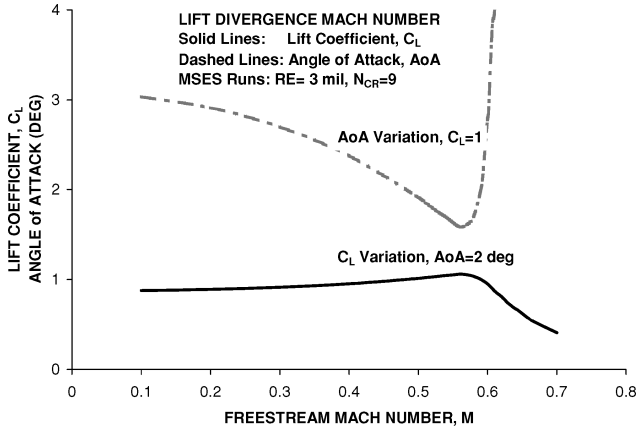

Fig. 11 Computed (MSES) lift coefficient and AOA variation with Mach number at $Re = 3 \times 10^6$ and $N_{cr} = 9$: ——, fixed $\alpha = 2$ deg and – – –, fixed $C_L = 1$.

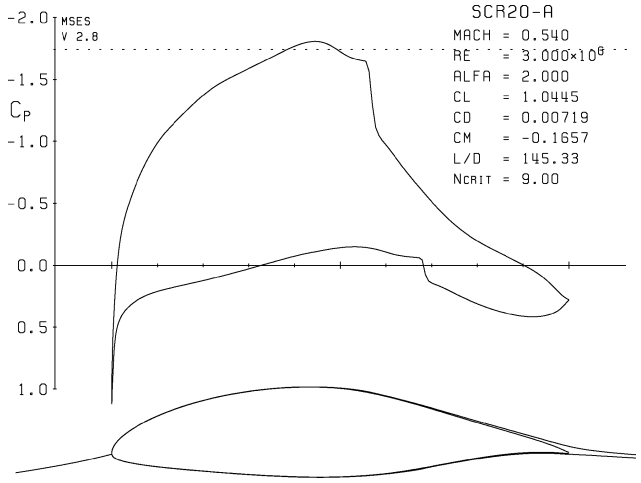

Fig. 12 Computed (MSES) surface pressure distribution for the SCR20-A airfoil exhibiting a critical Mach number of 0.54 and a critical pressure coefficient of -1.75, at $\alpha = 2$ deg, $Re = 3 \times 10^6$, and $N_{cr} = 9$.

The critical Mach number is of importance to determine the onset of shock formation for given angle-of-attack and flow conditions. Surface pressure data were obtained for various Mach numbers below M_D. As shown in Fig. 12, the critical pressure coefficient of -1.75 was predicted to be achieved at a critical Mach number of 0.54 for $Re = 3 \times 10^6$ and $\alpha = 2$ deg. As expected, this is slightly lower than the drag divergence Mach number of 0.58. When the wing sweep angle of 35 deg is considered, the SensorCraft wing, in fact, has a critical Mach number of 0.66 and a drag divergence Mach number of 0.70 (as opposed to the critical and divergence Mach numbers normal to the leading edge of 0.54 and 0.58 indicated, respectively, in this two-dimensional airfoil analysis). Notice also the very high value of lift-to-drag ratio of 145 for the airfoil shown in Fig. 12. In fact, the critical speeds set by the surface pressure distribution are not directly related to the drag or lift critical speeds.[19] This is mainly because the drag begins to increase anytime there is either supersonic flow or flow separation on any part of wing. If the flow separation does not occur at subcritical speeds, then there is no drag increase until reaching the critical Mach.

Figure 13 shows surface pressure distributions for Mach numbers ranging from 0.50 to 0.70 in increments of 0.04, including the data already presented in Fig. 12. At subcritical Mach numbers, the upper surface pressure has a gradual increase of negative pressures over the forward part probably until a point where the laminar separation bubble has its maximum thickness, followed by a pressure rise to the trailing edge. This is similar to the shape of roof-type pressure distributions, which delays critical Mach number by virtue

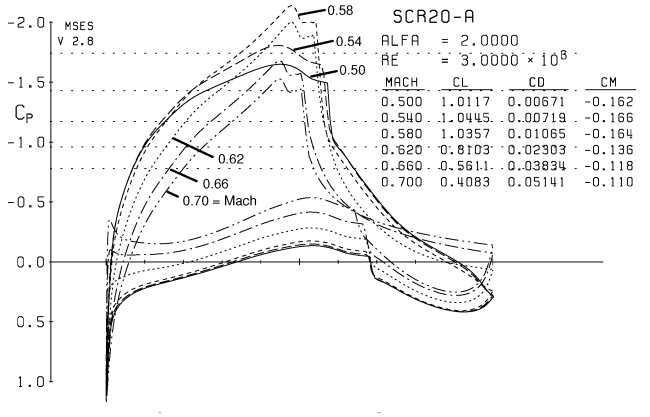

Fig. 13 Computed (MSES) surface pressure distributions for the SCR20-A airfoil at Mach numbers of 0.50, 0.54, 0.58, 0.62, 0.66 and 0.70, showing the effects of supercritical speeds at $\alpha = 2$ deg, $Re = 3 \times 10^6$, and $N_{cr} = 9$.

of a uniform velocity at the design condition (also Fig 6). As the Mach number increases beyond its critical value of 0.54, there is a dramatic change of surface pressures in the separation bubble region. The suction level basically moves to its maximum value at the supercritical Mach number of 0.58. This is probably due to the thickening of the boundary layer by the presence of locally supersonic flow embedded in the subsonic outer flow. The supersonic flow extends over a region in which there is near isentropic flow and shock-free compression waves. However, at Mach numbers above 0.58, the supersonic region is terminated by a normal shock and associated flow separation, which causes a decrease of not only the maximum suction pressure, but also a sharp decrease in lift and increase in drag coefficient, as shown in data tabulation of Fig. 13 and as was plotted in Figs. 10 and 11. Notice also the decrease in magnitude of pitching moment coefficient as the Mach number is raised above the drag divergence Mach.

Figure 14 shows the pressure contour to better illustrate shock formation and associated flow events at the same Mach number and flow conditions as the surface pressure distributions presented in Fig. 13. The shock formation is clearly visible in the dense region of pressure contours at the location of the separation bubble. Precompression waves are initially weak at Mach 0.54, but they get stronger with increase of Mach number and are terminated with a normal shock wave. They separate the laminar boundary layer well ahead of the first shock wave, which impinges on the free-shear layer and reflects as an expansion wave. The so-called shock-induced flow separation, clearly exhibited at Mach 0.62 and 0.66, limits the operational range of airfoils designed for HALE applications.

Airfoil Polars for SensorCraft

The SCR20-A airfoil performance was analyzed by using MSES for both design and the SensorCraft flow conditions presented in Table 1. This investigation included studies of polar performance and its sensitivity to various parameters including Reynolds number, Mach number, critical amplification factor, and wing loading.

The airfoil can operate at a cruise speed slightly above the critical Mach number. At this Mach number, there is a progress of shock-induced flow separation on the airfoil upper surface, as shown in pressure contour plots of Fig. 14. As Mach number is further increased, massive separation ensues. This shock induced separation is typically very unsteady, creating large fluctuations and excitation of the wing structure. This phenomenon is known as Mach buffet, and it imposes limitations on the operational flight regime. The airfoil should be brought to a lower altitude, where it would require a lower lift coefficient to maintain the same lift at a given Mach number. This would create a weaker shock and help avoid the Mach buffet. This type of deficiency in airfoil behavior is an off-design condition and clearly not acceptable. For a constant lift condition, the off-design may also be encountered with increasing altitudes as the aircraft weight decreases while consuming fuel in cruising flight.

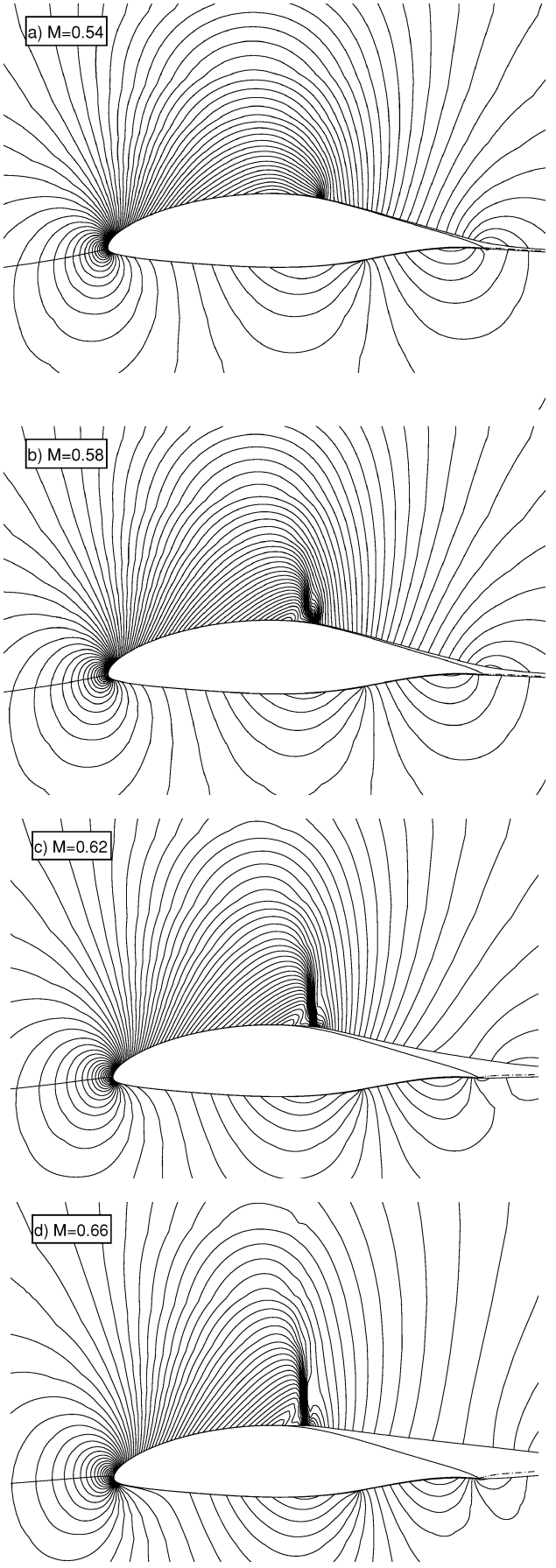

Fig. 14 Effects of the shock wave and its induced separation in pressure contours as the flow passes the critical flow condition; MSES predictions at $M = 0.54$, 0.58, 0.62, and 0.66, at $\alpha = 2$ deg, $Re = 3 \times 10^6$, and $N_{cr} = 9$.

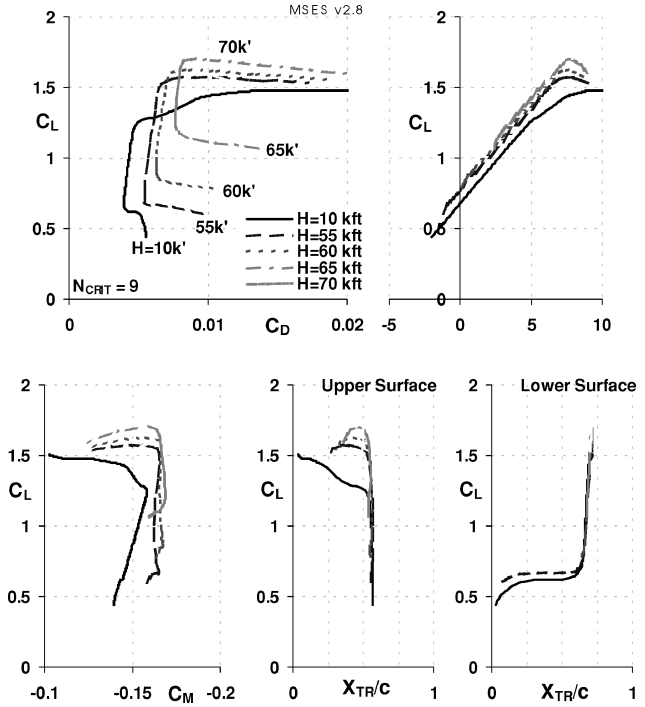

Fig. 15 Calculated (MSES) airfoil performance with constant lift M_R and Re_R parameters at 10,000-, 55,000-, 60,000-, 65,000-, and 70,000-ft altitude (M_R and Re_R parameter values as given in Table 1), $N_{cr} = 9$.

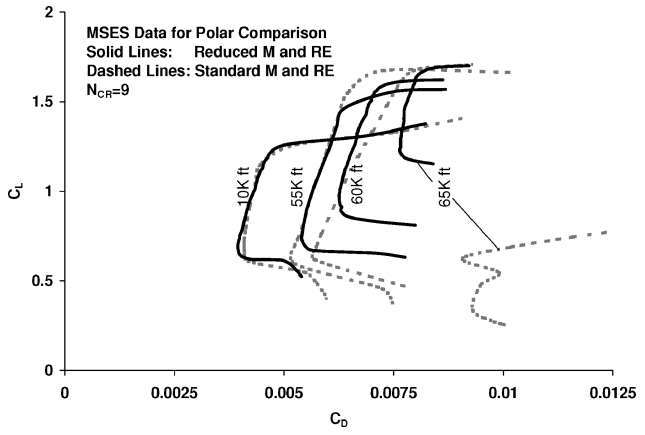

Fig. 16 MSES prediction of polars at 10,000-, 55,000-, 60,000-, and 65,000-ft altitudes, $N_{cr} = 9$, obtained by ——, constant lift M_R and Re_R parameters - - - -, holding standard Re and M constant.

To study the difference between the normal design and off-the design condition better, in Ref. 11 it is suggested to use of the constant-lift polar in which the reduced Mach number and reduced Reynolds number are held fixed, instead of the traditional Mach number and Reynolds number. Figure 15 shows the lift, drag, and pitching moment characteristics of the airfoil for SensorCraft altitudes of 10,000, 55,000, 60,000, 65,000, and 70,000 ft (at the corresponding reduced Reynolds and Mach numbers from Table 1 at takeoff maximum weight). The performance trends are similar to those presented earlier. The drag bucket clearly shifts upward with increasing altitude, and its operational (usable C_L) range becomes very narrow at 70,000 ft.

Figure 16 shows a comparison of these constant-lift drag polars at 10,000-, 55,000-, 60,000-, and 65,000-ft altitudes, with those obtained by holding standard Reynolds and Mach numbers constant. With increasing altitude, the constant-lift polars shift upward while the drag bucket of conventional polars expands over a larger range of lift coefficient with a decreasing slope ($\partial C_L/\partial C_D$). Each corresponding pair of polars for 10,000-, 55,000-, and 60,000-ft cases

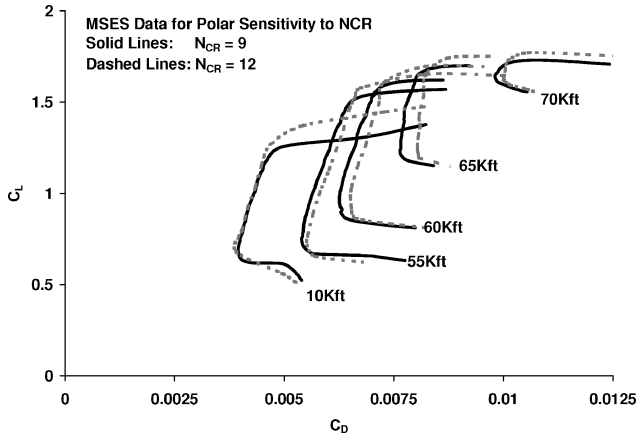

Fig. 17 MSES prediction of polar sensitivity to change in critical amplification ratios with M_R and Re_R parameters, given at 10,000-, 55,000,-60,000-, 65,000-, and 70,000-ft altitudes: ——, $N_{cr} = 9$ and - - - -, $N_{cr} = 12$.

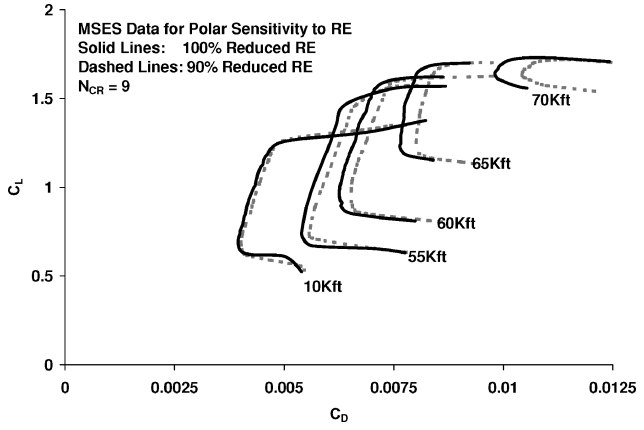

Fig. 18 MSES prediction of polar sensitivity to 10% decrease in Re_R at $N_{cr} = 9$ given at 10,000-, 55,000-, 60,000-, 65,000-, and 70,000-ft altitudes: ——, original Re_R and - - - -, Re_R decreased by 10%.

intersect at $C_L = 1$, where $M_R = M$ and $Re_R = Re$ by definition. There is a big difference between these polars at high altitudes near the ceiling condition for aircraft. The huge difference between polars at 65,000 ft is rather interesting because that makes this altitude operational for an off-the design condition for the airfoil, as opposed to what is considered to be an on-the design condition for the SensorCraft. However, accounting for the effect of the 35-deg wing sweepback could alleviate this situation because it brings the actual operating condition normal to the airfoil leading edge down to $M = 0.49$. The aircraft would have its maximum speed at the lower end of constant-lift drag buckets.

Given all of the uncertainties in design and analysis of the airfoil, it is important to evaluate the sensitivity of airfoil performance to the critical amplification ratio. For the present work, a critical amplification ratio of 9 was generally used for the e^N method. Figure 17 shows a comparison of the polars obtained for $N_{cr} = 9$ with those obtained for the $N_{cr} = 12$ case. The higher N_{cr} infers lower disturbance levels, more typical for HALE aircraft operating altitudes. However, the $N_{cr} = 12$ case produces higher drag values at higher altitudes, suggesting a delayed transition in the separation bubble. The delay is associated with a longer bubble that results in higher drag and maximum lift coefficient at altitudes. At higher altitude (lower Reynolds number), the change in the size of the separation due to N_{cr} is greater, resulting in a larger difference in the drag polars.

Figure 18 shows the polar sensitivity to 10% decrease in reduced Reynolds number at altitudes. When the Sensor Craft data are considered, 19% decrease in weight would in fact produce the 10% decrease in reduced Reynolds number for given altitude and aspect ratio. Because the reduced Reynolds number is inversely proportional

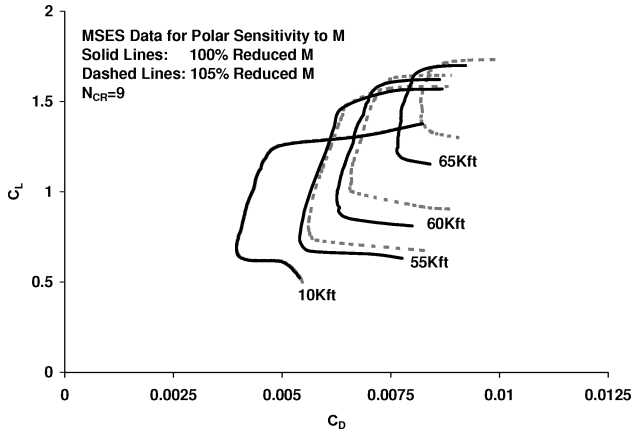

Fig. 19 MSES prediction of polar sensitivity to 5% increase in M_R at $N_{cr} = 9$ given at 10,000-, 55,000-, 60,000-, and 65,000-ft altitudes: ——, original M_R and - - - -, for M_R increased by 5%.

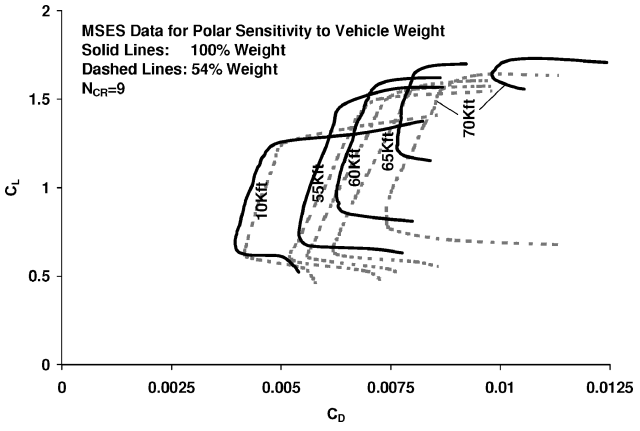

Fig. 20 MSES prediction of polar sensitivity to 46% a decrease in weight (due to fuel burn at end of loiter), at $N_{cr} = 9$, given at 10,000-, 55,000-, 60,000-, and 65,000–ft altitudes: ——, original takeoff weight and - - - -, weight decreased by 46%.

to aspect ratio, 20% increase in design aspect ratio produces the decrease in reduced Reynolds number for given altitude and aircraft weight. Increasing aspect ratio results in a decrease in induced drag, but it produces a greater increase in profile drag of wing that shows the overall drag increase at altitudes. The decrease in reduced Reynolds number has similar effects on the polar performance as those seen with the transition parameter and does not make significant difference in the operational range of the drag bucket with increasing altitudes.

Figure 19 shows the sensitivity of a 5% increase in reduced Mach number to the airfoil polars. Considering the Sensor Craft data, a 10% increase in wing loading would in fact produce the 5% increase in M_R for given altitude. The same effect is also true with aircraft gross weight, but this is shown in weight sensitivity analysis to follow. The increase in reduced M_R shifts the lower end of drag bucket upward while maintaining the maximum lift coefficients with an increase in the slope of drag bucket at increasing altitudes. The dramatic difference of polars at higher altitudes is quite obvious.

As can be seen from its definition, the parameter M_R would normally increase with increase of altitude for given wing loading in flight. Wing loading, in fact, decreases during the flight because of weight decrease with fuel burning. For the long flight duration, the SensorCraft is expected to consume about 40,000 lb of fuel, causing a 46% decrease in wing loading at the end of its long loiter time. The fuel-burn weight causes a reduction of 27% in both reduced Mach number and reduced Reynolds number parameters for given altitude, as shown with the data in Table 1. Figure 20 shows the polar sensitivity of the aircraft to this decrease in gross weight or wing loading. It is clear that there is a huge change of polar data with weight decrease. The drag bucket gets larger and shifts in the direction of lower lift coefficient with a decrease in its slope. The large difference is mainly attributed to the large reduction in reduced M_R. A comparison of Figs. 19 and 20 shows that whereas drag bucket shifts upward with a 5% increase in M_R, it shifts downward significantly with 27% decrease in M_R, although Fig. 20 also includes the effects of decrease in reduced Reynolds number. This shows the merits of designing an airfoil with a consideration of the flow conditions and configuration data established for an actual aircraft. The computational design, however, will better be validated with some wind-tunnel experiments.

Conclusions

A new 19.62% thick natural laminar flow airfoil, SCR20-A, was designed and analyzed for HALE applications. The geometry, weights, and operational altitudes of an in-house AFRL SensorCraft concept were used to define the design criteria for the airfoil. Sensitivity studies were carried out to determine the influence of reduced Reynolds number and Mach number, transition parameter, and weight on airfoil aerodynamic performance. The airfoil has the following typical design features.

1) There is laminar boundary-layer flow to about 60% chord upper and 70% chord lower surface, producing lift-to-drag ratios in the range of 145 at near the principle midcruise design condition. The transition location remains stable within the operational range of the drag bucket.

2) The transition is characterized by a laminar separation bubble, which decreases in size with increased of angle of attack as observed from the surface pressure distributions.

3) The airfoil has large drag bucket with a lift coefficient range of about 1.0. The range typically extends from maximum lift coefficient of 1.5 to a minimum value of 0.5 at which the airfoil may experience its maximum operational speed.

4) There is relatively low negative pitching moment in the range of -0.15 at $\alpha = 0$ deg, so that there is not much control required for longitudinal stability.

5) For the high thickness ratio, the airfoil has a drag divergence Mach number of 0.58 and critical Mach number of 0.54 at an angle of attack (AOA) of 2 deg and Reynolds number of 3×10^6. The critical speeds for the SCR20-A airfoil should be higher in case of its use for the SensorCraft concept due to its 35-deg wing sweepback.

Acknowledgments

The authors would like to acknowledge the support provided for this project by The U.S. Air Force Research Laboratory/Air Vehicle Directorate Summer Faculty Program, which the lead author participated in over the summers of 2001 and 2002 while on the faculty of Western Michigan University. We also acknowledge Mark Drela at Massachusetts Institute of Technology for providing his XFOIL and MSES codes.

References

[1]Johnson, F. P., "Sensor Craft: Tomorrow's Eyes and Ears of the Warfighter," AIAA Paper 2001-4370, Aug. 2001.

[2]Barbour, N., Bloxham, L., Fitzpatrick, C., Hunter, G., and Tapalian, C., "2001 Air/Space: The Year in Review: Sensor Systems," *Aerospace America*, Vol. 39, No. 12, Dec. 2001, pp. 50, 51.

[3]Mrozinski, D. P., Zeh, J. M., Reich, G. W., Carter, D. L., Cord, T. J., and Shenk, B., "Simulation-Based Research and Development; Technology Assessment Process," *Proceedings of the AeroSense 2002, SPIE—The International Society for Optical Engineering's 17th Annual Symposium on Aerospace/Defense Sensing, Simulation, and Controls*, Vol. 4716, Enabling Technologies for Simulation Science VI, edited by A. F. Sisti and D. A. Trevisani, 1–5 April 2002.

[4]Tyler, C., Schwabacher, G. J., and Carter, D., "Comparison of Computational and Experimental Studies for a Joined-Wing Aircraft," *Proceedings of the 40th Aerospace Sciences Meeting and Exhibit*, Reno, NV, Jan. 2002.

[5]Nangia, R. K., Palmer, M. E., and Tilmann, C. P., "Exploiting Unconventional Joined-Wing Concept For Subsonic & Supersonic Aircraft," *RTO-AVT-099, Symposium on Novel and Emerging Vehicle and Vehicle Technology Concepts*, Brussels, Belgium, 7–11 April 2003.

[6]Blair, M., and Canfield, R. A., "A Joined-Wing Structural Weight Modeling Study," *Proceedings of the 43rd AIAA/ASME/ASCE/AHS/ASC Structures, Structural Dynamics, and Materials Conference*, Denver, CO, April 2002.

[7]Reich, G., Raveh, D., and Zink, P., "Application of Active Aeroelastic Wing Technology to a Joined-Wing SensorCraft," *Proceedings of the 43rd AIAA/ASME/ASCE/AHS/ASC Structures, Structural Dynamics, and Materials Conference*, Denver, CO, April 2002.

[8]Nangia, R. K., Palmer, M. E., and Tilmann, C. P., "On Design of Unconventional High Aspect Ratio Joined-Wing Type Aircraft Configurations," International Council of the Aeronautical Sciences, Toronto, Canada, Sept. 2002.

[9]Nangia, R. K., Palmer, M. E., and Tilmann, C. P., "Unconventional High Aspect Ratio Joined-Wing Aircraft Incorporating Laminar Flow," AIAA Paper 2003-3927, June 2003.

[10]Nangia, R. K., Palmer, M. E., and Tilmann, C. P., "Unconventional High Aspect Ratio Joined-Wing Aircraft with Aft- and Forward-Swept Wing-Tips," AIAA Paper 2003-0605, Jan. 2003.

[11]Drela, M., "Transonic Low-Reynolds Number Airfoils," *Journal of Aircraft*, Vol. 29, No. 6, 1992, pp. 1106–1113.

[12]Torenbeek, E., *Synthesis of Subsonic Airplane Design*, Delft Univ. Press, Kluwer Academic, Delft, The Netherlands, 1982, pp. 241–252.

[13]Greer, D., Hamory, P., Krake, K., and Drela, M., "Design and Predictions for a High-Altitude (Low Reynolds Number) Aerodynamic Flight Experiment," AIAA Paper 99-3183, June 1999.

[14]Drela, M., "A User's Guide to MSES 2.8," Computational Aerospace Sciences Lab., Massachusetts Inst. of Technology, Cambridge, MA, May 1995.

[15]Tilmann, C. P., Brandt, L. B., Russell, W. J., Ramsay, R. R., and Höhn, T., "Development and Validation of Airfoils for Global Range Transports," *Proceedings of the 18th AIAA Applied Aerodynamics Conference*, Denver, CO, Aug. 2000.

[16]Tilmann, C. P., "Enhancement of Transonic Airfoil Performance Using Pulsed Jets for Separation Control," *Proceedings of the 39th AIAA Aerospace Sciences Meeting and Exhibit*, Reno, NV, Jan. 2001.

[17]Selig, M. S., Maughmer, M. D., and Somers, D. M., "Natural Laminar Flow Airfoil for General Aviation Applications," *Journal of Aircraft*, Vol. 32, No. 4, 1995, pp. 710–715.

[18]Maughmer, M. D., and Somers, D., "Design and Experimental Results for a High-Altitude, Long-Endurance Airfoil," *Journal of Aircraft*, Vol. 26, No. 2, 1989, pp. 148–153.

[19]Perkins, C. D., and Hage, R. E., *Airplane Performance Stability and Control*, Wiley, New York, 1949, pp. 44–49.